

LA-UR-

11-04390

Approved for public release;
distribution is unlimited.

Title: Shock compression and spallation of single crystal tantalum

Author(s): Q. An, Ravelo, T. C. Germann, W. Z. Han, S. N. Luo, D. L. Tonks, W. A. Goddard III

Intended for: The 17th APS Shock Compression of Condensed Matter, Chicago, June 26–July 1, 2011, conference proceedings



Los Alamos National Laboratory, an affirmative action/equal opportunity employer, is operated by the Los Alamos National Security, LLC for the National Nuclear Security Administration of the U.S. Department of Energy under contract DE-AC52-06NA25396. By acceptance of this article, the publisher recognizes that the U.S. Government retains a nonexclusive, royalty-free license to publish or reproduce the published form of this contribution, or to allow others to do so, for U.S. Government purposes. Los Alamos National Laboratory requests that the publisher identify this article as work performed under the auspices of the U.S. Department of Energy. Los Alamos National Laboratory strongly supports academic freedom and a researcher's right to publish; as an institution, however, the Laboratory does not endorse the viewpoint of a publication or guarantee its technical correctness.

SHOCK COMPRESSION AND SPALLATION OF SINGLE CRYSTAL TANTALUM

Q. An^{*†}, R. Ravelo^{†}, T. C. Germann[†], W. Z. Han[†], S. N. Luo[†], D. L. Tonks[†] and W. A. Goddard, III^{*}**

^{}Materials and Process Simulation Center, California Institute of Technology,
Pasadena, California 91125, USA*

[†]Los Alamos National Laboratory, Los Alamos, New Mexico 87545, USA

*^{**}Department of Physics, University of Texas at El Paso, El Paso, Texas 79968, USA*

Abstract. We present molecular dynamics simulations of shock-induced plasticity and spall damage in single crystal Ta described by a recently developed embedded-atom method (EAM) potential and a volume-dependent qEAM potential. We use impact or Hugoniotostat simulations to investigate the Hugoniots, deformation and spallation. Both EAM and qEAM are accurate in predicting, e.g., the Hugoniots and γ -surfaces. Deformation and spall damage are anisotropic for Ta single crystals. Our preliminary results show that twinning is dominant for [100] and [110] shock loading, and dislocation, for [111]. Spallation initiates with void nucleation at defective sites from remnant compressional deformation or tensile plasticity. Spall strength decreases with increasing shock strength, while its rate dependence remains to be explored.

Keywords: Spallation, twinning, dislocation, shock, bcc

PACS: 62.50.Ef, 61.72.-y

INTRODUCTION

Body-centered cubic (bcc) metals, e.g., Ta, W, Mo and Nb, are of great interest both for condensed matter physics and materials science and engineering. However, experimental data and simulations of their physical and mechanical properties under extreme conditions are scarce. Our abilities to predict deformation, damage and phase transitions (if any) in bcc metals under high strain-rate loading are limited by, e.g., the lack of accurate and readily implementable interatomic potentials. A more detailed discussion of various Ta potentials in particular can be found in R. Ravelo *et al.* in this proceedings.

Here we perform molecular dynamics (MD) simulations to examine the accuracy of some recently developed potentials of simple forms (embedded-atom-method or EAM potentials) as regards shock loading, and to investigate deformation and spall damage under shock loading as well as the related mecha-

nisms. Two EAM potentials are of particular interest: one by R. Ravelo *et al.* (this proceedings) simply denoted as EAM, and the other by Strachan *et al.* denoted as qEAM[1]. We show that both potentials reproduce the experimental Hugoniots, and reveal the anisotropic deformation and damage processes in single crystal Ta.

METHODOLOGY

The Ta EAM potential adopts the standard EAM form (R. Ravelo *et al.*, this proceedings), while for the qEAM potential, the electron density depends on the local volume or mass density[1]. Such volume dependence may be a concern for the later stage of spallation (large voids), so we choose not to perform direct spall simulations with qEAM. We compute the γ -surfaces $\langle 111 \rangle \{112\}$ and $\langle 100 \rangle \{110\}$ for both po-

tentials (not shown), which reproduce the density-functional theory calculations. Direct impact simulations are performed with EAM, and the Hugoniotostat simulations, with qEAM. For spallation simulations, we use the flyer plate–target configuration, where the length of the flyer plate is half of that of the target. The equivalent shock-state particle velocity is denoted as u_p . More details were presented elsewhere[2] for impact simulations.

We explore three main crystallographic directions as the shock loading direction (the x -axis): [100], [110] and [111]. The system sizes are $\sim 1,000,000$ atoms, and the dimensions, are $\sim 100 \times 13 \times 13 \text{ nm}^3$. Periodic boundary condition is applied in three dimensions for the Hugoniotostat simulations, but not along the shock direction for the impact simulations. The time step for integrating the equation of motion is 1 fs, and the run durations are up to 60 ps. We perform one-dimensional (1D) binning analysis[2] to obtain the shock profiles of some physical properties such as stress tensor (σ_{ij}). The atomic von Mises shear strain (η^{vM}) analysis is used for resolving local deformation [3].

RESULTS AND DISCUSSION

For the flyer plate–target impact, the shock compression waves are reflected at the free surfaces of the flyer and target as the release fans, which propagate backward into the flyer and target, unload the material and lead to an evolving tensile region in the target. At sufficient shock strength, spallation occurs. Such compression, unloading and tension processes are illustrated in the position–time ($x-t$) diagram in terms of local density (Fig. 1). For the Hugoniotostat simulations, we apply compression under the 1D strain condition without wave propagation, and deduce shock properties from the jump conditions. We explore u_p up to 2.5 km/s.

We first examine the behavior of Ta single crystals under shock compression. In the impact simulations, we observe evident elastic-plastic (two-wave) structure for [111] loading, while the elastic-plastic transition is less pronounced for [100] loading, and it is not identifiable for [110] loading. Fig. 1 shows an example for [111] loading. Much large system sizes are likely needed for obtaining well defined transition profiles. (Some such studies are presented in R.

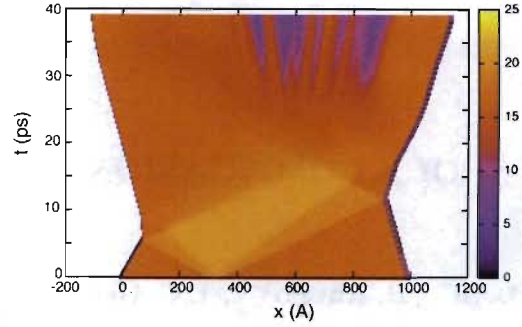


FIGURE 1. The $x-t$ diagram for the $\langle 111 \rangle$ shock loading at $u_p=1$ km/s, color-coded with density in g/cm^3 . The impact plane is at $x \sim 330 \text{ \AA}$. The elastic and plastic shocks, free surface release fans, and the spall zones (blue) are evident.

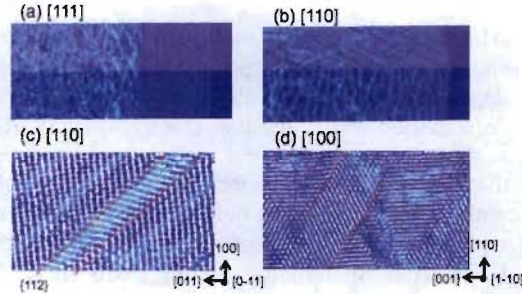


FIGURE 2. Shock-induced plasticity in Ta at $u_p=1$ km/s for different loading orientations: dislocations (a) and twinning (b–d). The dashed lines denote the twin planes $\{112\}$, and the area between them, a twin band. Shock direction: from left to right. Color coding is based on η^{vM} .

Ravelo *et al.* in this proceedings.) Therefore, we do not extract the exact shock parameters in the two-wave regime, since there exists ambiguity in applying the jump conditions; we focus on the deformation mechanisms in this regime instead (Fig. 2).

The slip systems in bcc metals are $\langle 111 \rangle \{110\}$, $\langle 111 \rangle \{112\}$ and $\langle 111 \rangle \{123\}$. Upon shock compression, the Ta single crystals show different deformation behaviors. The results from EAM and qEAM are similar so we show only those for the former (Fig. 2). For the shock states at $u_p=1$ km/s, we observe dislocations in the case of [111], and twinning, [110] and [100]. For [111], the dislocations may have both edge and screw contributions [Fig. 2(a)] but the exact nature remains to be resolved. For [110], well-defined

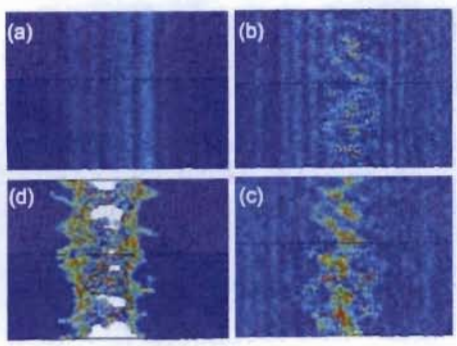


FIGURE 3. Snapshots of tensile plasticity, and void nucleation and growth for [110] loading at $u_p=0.5$ km/s. (a): 21 ps; (b): 22 ps; (c): 23 ps; (d): 25 ps.

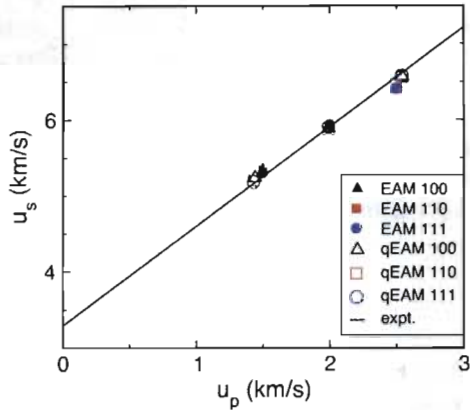


FIGURE 4. The u_s-u_p relations for the plastic wave predicted from the EAM and qEAM potentials, compared to experiments [4]. The results for qEAM are from Hugoniotostat simulations.

twins are evident [Figs. 2(b) and 2(c)], and the $\{111\}\{112\}$ system is activated. The region bound by two neighboring $\{112\}$ twin planes forms a twin band, which along with the $\{011\}$ planes produce a zig-zag structure typical of twinning [Fig. 2(c)]. Twinning is similar for the [100] shock. However, deformation mechanisms may depend on exact nature of loading, e.g., plastic deformation may not be symmetric with respect to compression and tension. For [110] loading at $u_p=0.5$ km/s, the crystal remains elastic upon shock, but it shows certain localized dislocation-like deformation during tension right before spallation (Fig. 3; also see discussion below on spallation).

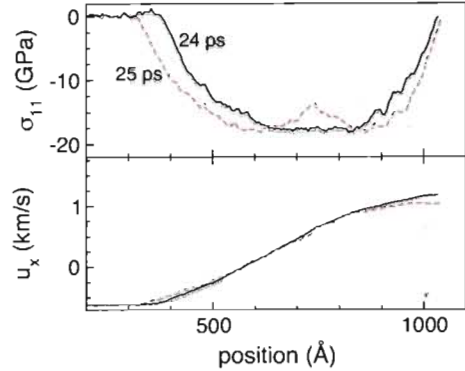


FIGURE 5. Stress and particle velocity profiles for the [110] loading at $u_p=1$ km/s near the onset of spallation.

At sufficient shock strength, the plastic shock overtakes the elastic precursor. In this single plastic wave regime, we deduce the shock parameters from the jump conditions or directly from the wave profiles. Fig. 4 shows the MD simulations of the u_s-u_p relation in comparison with the experiments[4]. (u_s denotes shock velocity.) Both potentials (EAM and qEAM) and both shock simulations approaches (direct impact and Hugoniotostat) yield the results in excellent agreement with the experiments. There no anisotropy in the Hugoniots in this regime as expected.

The interactions of the two release fans may lead to tensile stress σ_{xx} in the target above a critical value, σ_{sp} , leading to spallation (Figs. 1, 3 and 5). Spallation can be identified from the $x-t$ diagrams, in-volume profiles (Fig. 5) and free surface velocities, e.g., as rapid density reduction, temperature increase, and pullback in stress or free surface velocity. In our spall simulations, u_p ranges from 0.4 km/s to 1 km/s. The stress and particle velocity profiles (Fig. 5) right before spall (nanovoid nucleation) allow for σ_{sp} (or the maximum tensile stress) and tensile strain rate to be determined[2]. The tensile strain rate range explored with the direct impact method is limited, about 10^9-10^{10} s $^{-1}$ in our simulations.

Fig. 6 compares the spall strength for the three loading orientations. σ_{sp} is highly anisotropic for $u_p<1$ km/s. For the system sizes (the flyer and target lengths) explored, spallation occurs at $u_p\geq 0.65$ km/s, 0.45 km/s, and 0.6 km/s for $\langle 100 \rangle$, $\langle 110 \rangle$, and $\langle 111 \rangle$, respectively. For low u_p where compression plasticity can be negligible, the critical tensile stress dif-

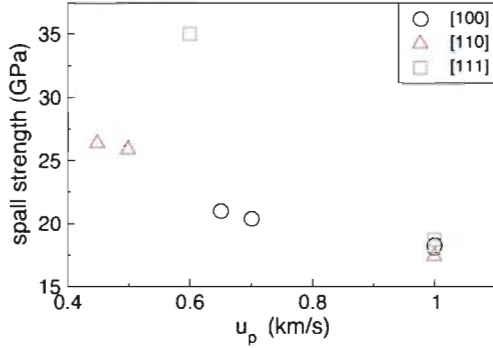


FIGURE 6. Spall strength vs. shock strength (u_p) for different orientations. The lowest u_p is the lower limit for spallation to occur.

fers drastically (in decreasing order: [111], [110] and [100]), due to the anisotropic wave speed and yield behavior (compression and tension). With increasing shock strength, the anisotropy in the spall strength decreases and it is essentially the same at $u_p=1$ km/s. This is caused by increased shock heating, and compressional and tensile plasticity that smear the microstructure difference for different loading orientations, and thus, anisotropy in spall damage, consistent with our observations on single crystal Cu[2]. In experiments, a substantially lower spall strength of 7.3 GPa was reported[5]; both strain rate and microstructure effects are likely the reasons for the discrepancy.

The early stage of spallation is essentially nanovoid nucleation, and the underlying mechanism is interesting. We choose a low velocity impact case where the damage is small or close to incipient spall ($u_p=0.5$ km/s for [110]; Fig. 3). In this case, the crystal remains elastic during shock compression and subsequent release. With increasing tension, the tensile region sequentially shows increasing shear but remains elastic [Fig. 3(a)], local plastic deformation [Fig. 3(b)], void nucleation at highly sheared sites [Fig. 3(c)], and void growth and coalescence [Fig. 3(d)]. Thus, plastic deformation or defect formation associated with it are prerequisite for void nucleation. In the case compression plasticity is partially preserved, it couples with tensile plasticity and they contribute collectively to defect formation for void nucleation. During void growth, the shear deformation in the region immediately around a void may be recovered due to the stress relaxation.

This void nucleation and growth process and its interaction with shear deformation are similar in other single crystal metals such as Cu[6]. Since defect formation (e.g., plasticity) is necessary for void nucleation and coupled with void growth, the rate dependence of spall damage is coupled with that of local deformation, which in turn strongly depends on microstructure.

CONCLUSION

We characterize shock compression and spallation of Ta single crystals with MD simulations and accurate EAM and qEAM potentials. Deformation and spall damage are anisotropic for Ta single crystals. Our preliminary results show that twinning is dominant for [100] and [110] shock loading, and dislocation, for [111]. Spallation initiates with void nucleation at defective sites from remnant compressional deformation or tensile plasticity. Spall strength decreases with increasing shock strength, while its rate dependence remains to be explored.

ACKNOWLEDGMENTS

We have benefited from discussions Y. Z. Tang. This work was supported by the LDRD and ASC programs at LANL, and the PSAAP project at Caltech.

REFERENCES

1. Strachan, A., Çağın, T., Gulseren, O., Mukherjee, S., Cohen, R. E., and Goddard III, W. A., *Model. Sim. Mat. Sci. Eng.*, **12**, S445 (2004).
2. Luo, S. N., An, Q., Germann, T. C., and Han, L. B., *J. Appl. Phys.*, **106**, 013502 (2009).
3. Shimizu, F., Ogata, S., and Li, J., *Mater. Trans.*, **48**, 2923–2927 (2007).
4. Marsh, S. P., *LASL Shock Hugoniot Data*, University of California Press, Berkely, 1980.
5. Zurek, A. K., Thissel, W. R., Johnson, J. N., Tonks, D. L., and Hixson, R., *J. Mater. Process. Tech.*, **60**, 261 (1996).
6. Luo, S. N., Germann, T. C., and Tonks, D. L., *J. Appl. Phys.*, **107**, 056102 (2010).